Indonesian Journal of Chemical Research

http://ojs3.unpatti.ac.id/index.php/ijcr Indo. J. Chem. Res., 13 (1), 38-45, 2025

Synthesis, Microstructure, Optical Properties, and Sensitive Amoxicillin Detection of Carbon Dots

Yuni Aldriani Lubis [1], Saharman Gea[2], Muhammad Frassetia Lubis[3], Woei Wu Larry Pai[3], Marpongahtun[2]*

[1]Postgraduate School, Department of Chemistry, Faculty of Mathematics and Natural Sciences, Universitas Sumatera Utara, Jl. Bioteknologi No.1, Medan, 20155, Indonesia

[2]Department of Chemistry, Faculty of Mathematics and Natural Sciences, Universitas Sumatera Utara, Jl. Bioteknologi No. 1 Medan, 20155, Indonesia

[3]Center for Condensed Matter Sciences, National Taiwan University, No. 1, Sec. 4, Roosevelt Road, Taipei, 10617, Taiwan

Corresponding Author: marpongahtun@usu.ac.id

Received: March 2025
Received in revised: April 2025
Accepted: May 2025
Available online: May 2025

Abstract

The detection of amoxicillin has been successfully carried out using C-dot fluorescence probes made from d-glucose and urea. The fluorescence probe has an intense bright blue emission under UV light at 395 nm and and depends on the excitation and depends on the excitation. The PL decay study was evaluated and has a lifetime decay of 4.09 ns. Raman studies successfully showed a D peak at 1381 cm^{-1} and a G peak at 1586 cm^{-1} associated with the presence of graphitic and amorphous structures. The absorption peaks in UV-vis spectroscopy confirm transitions at 275 nm ($\pi \rightarrow \pi^*$) and 322 nm ($n \rightarrow \pi^*$) with the presence of conjugated C=C and carbonyl (C=O) functional groups. The results of the fluorescence test show a bright blue color, with its intensity measured at an excitation of 365 nm. This can be attributed to nitrogen incorporation on the surface of the C-dots derived from urea, resulting in a quantum yield (QY) of 54%. This fluorescence probe is highly sensitive in detecting amoxicillin (AMX), as evidenced by the successful detection of AMX at concentrations of 10–30 μM and a resulting LOD of 5.75443×10−7 nM. The microstructure of C-dots shows a uniform size of C-dot nanoparticles, and C-dot modeling was created. C-dot probes have an LOD of 5.75443×10^{-7} nM, indicating high sensitivity in detecting AMX.

Keywords: C-dots, Microstructure, Hydrothermal, Raman Spectroscopy, AMX, Optical Properties

INTRODUCTION

Amoxicillin (AMX) is an antibiotic used to treat infectious diseases caused by bacterial infections due to pathogenic bacteria with gram-positive and gram-negative bacteria. This antibiotic has strong antibacterial properties and can penetrate the cell membrane. AMX is a type of semi-synthetic β-lactam penicillin antibiotic (Attia, Nassar, El-Zeiny, & Serag, 2016; Guo, Dong, Chen, & Chen, 2022; Jessy Mercy et al., 2023; G. Yang & Zhao, 2015). AMX is extensively utilized in humans, livestock, and aquaculture as a disease-prevention medication. The low metabolism rate of AMX in the body, around 70 – 90%, results in a significant amount being released by the body through urine and feces, exposing the environment (Verma, Aggarwal, Singh, Sharma, & Sarma, 2022; Ye, Chen, Tang, Sun, & Song, 2025).

AMX has been detected in river water, seawater, and other aquatic environments, posing a danger if consumed by humans and other organisms. Even after water treatment and recycling, it still cannot be fully identified, so many methods and technologies continue to be offered to identify AMX in water (Jessy Mercy et al., 2023). Consequently, it is critical to use various analytical methods to find traces of AMX in water. Because of its low cost, simplicity, quick reaction, ease of use, and high sensitivity, AMX detection using carbon dots probes has emerged as one of the most used techniques (Ye et al., 2025).

Carbon dots (C-dots) are spherical nanoparticles with sizes less than 10 nm. C-dots have several advantages, including excellent biocompatibility, easy availability, and good optical properties (Jiang et al., 2025; Liu et al., 2024). However, C-dots usually exhibit poor optical properties if not doped with heteroatoms. Heteroatom doping, such as with chlorine (Cl), nitrogen (N), boron (B), sulfur (S), and oxygen (O), can enhance the optical properties of C-dots (Barus, Ginting, Faizah, Shafira, & Nainggolan, 2023; Mallik et al., 2025).

Because nitrogen and carbon have similar atomic sizes, nitrogen (N) is an intriguing dopant. N-doping increases active sites and fluorescence while not substantially changing the electrical structure (Wu, Zeng, Zheng, You, & Liu, 2025). Nitrogen doping of C-dots will enhance the quantum yield measured by a photoluminescence spectrometer (Marpongahtun et al., 2023). Several studies related to nitrogen doping of C-dots have been conducted.

Akbar et al. (2025) synthesized N – CD from oxalic acid and malic acid as precursors, rare earth metal salts and diammonium tartrate as doping and nitrogen sources. The solvothermal/hydrothermal approach was used to perform the synthesis. The results showed that the N – CD probe exhibited a linear relationship when plotted with alpha-fetoprotein (AFP) concentrations from 0.01 to 3.0 ng/mL, indicating good sensitivity and high quantitative sensor accuracy. Cai et al. (2025) conducted a study on N-CQD synthesis using the hydrothermal method sourced from pumpkin and melamine to detect nifuratel and temperature. The result is that N-CQD is very sensitive because it can detect within a linear range of 0.5–100 μM and an LOD of 0.074 μM. Then, Ye et al. (2025) synthesized N, S-CDs@MIP to detect AMX using the hydrothermal method. The result is a highly sensitive probe that successfully detected AMX with a detection limit of 1.17 ng/mL, a linear range of 5.8–200 ng/mL, and an RSD of <3%.

Thus, in contrast to previous studies that employed complex precursors or multi-step doping strategies, this study presents a simple, environmentally friendly, and cost-effective approach to synthesize nitrogen-doped carbon dots (N-CDs) from d-glucose and urea via a hydrothermal method. D-glucose is a carbohydrate compound with a hydroxyl functional group (-OH). The -OH group can be converted into an ester through an esterification reaction. D-Glucose is a potential material because it has a sufficient number of C bonds (as many as 6).(Dali, Dali, Dali, & Amalia, 2021). The developed C-dots exhibited excellent optical properties, high quantum yield of 54%, and very low detection limit of 5.75443×10^{-7} nM for amoxicillin (AMX) sensing. This demonstrates the potential of these C-dots as highly sensitive, sustainable, and scalable probes for antibiotic detection in environmental samples.

METHODOLOGY

Materials and Instrumentals

This experiment used analytical grade reagents and deionized water (electrical reactivity of 0.5 MΩ.cm and conductivity of 2.0 μS/cm). D-glucose monohydrate precursor, urea (nitrogen source), Whatman filter paper were purchased from CV. Rudang Jaya, Indonesia. The syringe filter 0.22 μm was obtained from Sigma-Aldrich. All materials were used without further purification.

Characterization of C-dots was recorded by UV-Vis Spectroscopy (Shimadzu UV-1900i), and Photoluminescence C-dots were recorded by Microplate Reader BioTek Synergy H1 (Agilent Technologies). HORIBA recorder Raman - The LabRAM HR Evolution Raman Microscopes using a laser beam 532 nm. The microstructure image was verified by Microscope Leica 247601, APO PL 20x 0.45 Germany Vistech.

C-dots Synthesis

C-dots were synthesised using a straightforward hydrothermal process and slight modification (Amin et al., 2025). Initially, 30 mL of deionized water was used to dissolve 3 g of d-glucose monohydrate. The dispersed solution was then stirred with a hotplate for 30 minutes to obtain homogeneity. The solution that was being stirred was added with 1.55 g of urea until it dissolved completely and produced a clear color solution. A 100 mL autoclave was filled with this clear solution. For 8 h, the autoclave was heated to 180 ^{o}C in the oven. The autoclave was then left to stand for a day. After collecting the solution, it was centrifuged for 30 minutes at 5500 rpm. Whatman no. 42 filter paper and a 0.22 μm syringe filter were used to filter the resulting supernatant. The solution was gathered for later use and kept at 4 ^{o}C in a refrigerator. The C-dots solution was characterized by PL, UV-Vis, Raman, and irradiated with UV lamp 395 nm.

Amoxicillin Detection

Amoxicillin (AMX) detection was performed using the fluorescence method, where C-dots were at 365 nm excitation. First, a stock solution was prepared. Antibiotic solutions were prepared with of 10, 15, 20, 25 and 30 μM concentrations. Then, the solution was added with 10 μL of C-dots up to the maximum volume limit of 10 mL and sonicated for 10 minutes until the solution was homogeneous and completely dissolved (Mousa, Abdelrahman, Fahmy, Ebrahim, & Moustafa, 2023).

Quantum Yield

The quantum yield (QY) calculation begins by diluting C-dots in deionized water with a refractive index (η) of 1.33. Quinine sulfate is used as the standard fluorescence reference (QY=54%), which is

diluted in 1M H_2SO_4. C-dot and quinine sulfate solutions were prepared (absorbance 0.05) at an excitation of 365 nm, and measurements were conducted using a quartz cuvette (size: 1 cm). The calculation of quantum yield (QY) uses the following equation:

$$QY_m = QY_n \left(\frac{A_n}{A_m}\right)\left(\frac{I_m}{I_n}\right)\left(\frac{\eta_m^2}{\eta_n^2}\right) \quad (1)$$

From that equation, QY indicates the quantum yield from that equation, η is the solvent refractive index, A is the absorbance, and I is the PL intensity at 365 nm. Symbols of m and y refer to C-dots and quinine sulfate. QY can be calculated accurately (Akbar et al., 2025).

RESULTS AND DISCUSSION

Photoluminescence

Using PL spectrometer, C-dots will be measured for emission intensity with excitation (365 nm). This characterization is done to study the optical characteristics of C-dots. This technique also plays a significant role in calculation of quantum yield (Mansuriya & Altintas, 2018). The PL spectrum displays photoluminescence emission in the range of 400–700 nm. Figure 1. C-dots have a central emission peak at 450 nm, indicate blue emission when excited. This is because the presence of asymmetrically stretched oxygen atoms connecting nitrogen atoms affects the emission peak (Marpongahtun et al., 2018; J. Yang, Wang, & Lu, 2025).

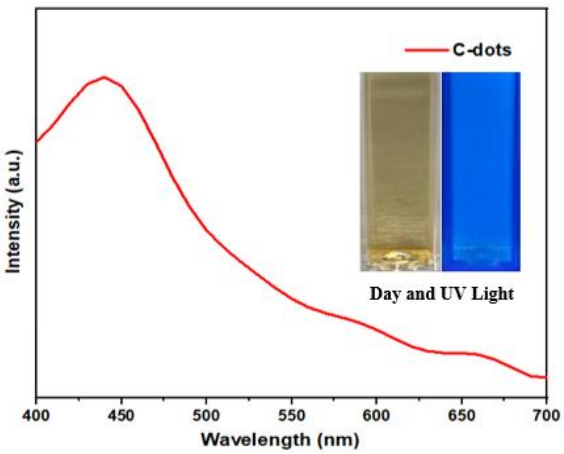

Figure 1. Photoluminescence spectra of C-Dots (365 nm)

The PL characterization results are also supported by physical images of luminescence produced by C-dots. The C-dots exhibited blue fluorescence, with an emission peak at 440 nm, upon irradiation of the aqueous solution containing C-dots with a UV lamp 395 nm. The blue emission resulting from UV lamp irradiation and the emission peak at 440 nm in a phenomenon that is compatible with the

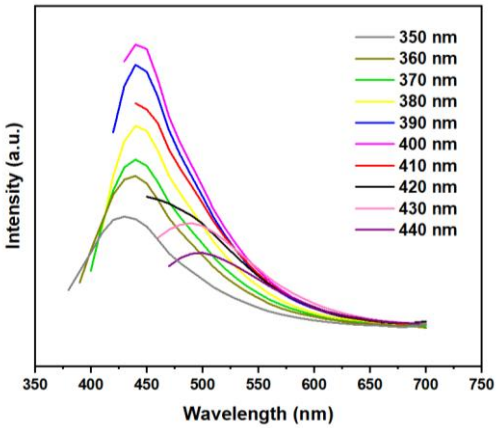

Figure 2. PL spectra of C-Dots in different excitation

surface defect state's absorption peak is shown by PL analysis. (Chu et al., 2025).

In Figure 2 above, it can be observed that the fluorescence intensity depends on the excitation. After conducting tests with different wavelength variations, different intensities were obtained. This is associated with a significant redshift and a decrease when the excitation increases, caused by quantum effects and surface defects (Sanni et al., 2025; Sun et al., 2023).

Time-Resolved Photoluminescence

Further characterization was carried out using Time-resolved photoluminescence (TRPL) with the aim of investigating the fluorescence decay behavior of the synthesized C-dots. As shown in Figure 3, the fluorescence intensity of the C-dots decreases sharply in the first few hundred nanoseconds and gradually levels off, exhibiting a characteristic biexponential decay profile. The PL decay curve was calculated using the following equation:

$$y = A_1 \exp\left(\frac{-x}{\tau 1}\right) + A_2 \exp\left(\frac{-x}{\tau 2}\right) + y_0 \quad (1)$$

Meanwhile, the average of PL decay is calculated using the following formula.

$$\tau_{Average} = \sum_{n=1}^{2} \frac{A_n \tau_n^2}{A_n \tau_n} \quad (2)$$

Based on the equation above, it is known that the decay time of N-CDs calculated from the equation above is 4.09 ns. Monitoring emission at specific wavelengths concludes that the reorientation of the

environmental molecular dipole towards the emitter dipole depends on the surface polarity of N-CDs and the polarity of the solvent, resulting in emission from the relaxed sub-state of N-CDs that becomes filled. Furthermore, when the excited state lifetime of the emitter is sufficiently long and longer than the solvent relaxation time, the maximum light emission experiences a redshift as a function of time. Therefore, monitoring PL emission at longer wavelengths will result in a more delayed maximum formation. (Dimitriev et al., 2024).

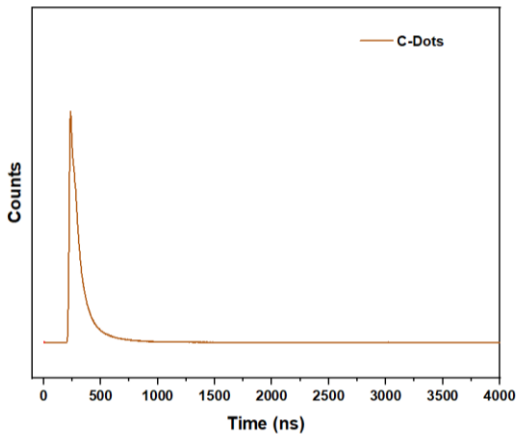

Figure 3. TRPL of C-Dots

Raman Spectroscopy

A non-invasive and non-destructive technique for figuring out the state of carbon in C-dots is Raman spectroscopy. This method provides information on two bands, the D and G bands, where the G band indicates the existence of flaws or abnormalities in the carbon structure and the D band indicates the presence of graphitic structures (Khairol Anuar, Tan, Lim, So'aib, & Abu Bakar, 2021; Mansuriya & Altintas, 2018; Saraswat & Yadav, 2020; Zaib, Akhtar, Maqsood, & Shahzadi, 2021). The two peaks in Figure 4 at 1381 cm^{-1} and 1586 cm^{-1} are ascribed to the D bands in C-dots, which show the number of defects on the sp^3 surface, and the G bands, which show the sp^2 gravity. The peak at 1586 cm^{-1} indicates high crystallinity properties with sp^2 hybridization; the other, at 1381 cm^{-1} indicates impurities (Murugan et al., 2025).

The microstructure of C-dots clarifies the structural state of C-dots with 50x magnification. Figure 5 shows the variation in the topographic structure and microstructure of C-dots. The G band (1586 cm^{-1}) shows an area with a more uniform texture of C-dot particles, and the intensity is higher than the D band (1381 cm^{-1}). Meanwhile, the irregular

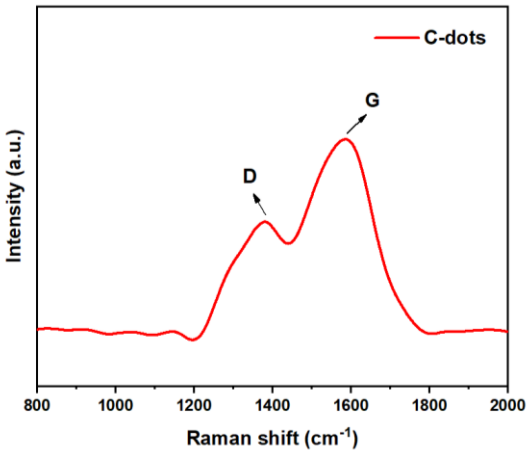

Figure 4. Raman spectra of C-Dots

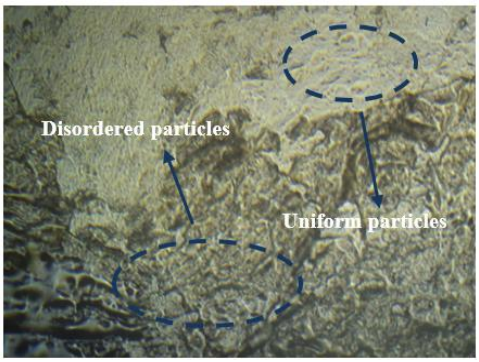

Figure 5. Microstructure of C-Dots

morphology, numerous defects, and irregularities and the possible presence of larger particles in the surrounding area tend to originate from the G band associated with graphitization (Akbar et al., 2025).

UV-vis Spectroscopy

UV-vis spectroscopy is a proper characterization to determine the absorption wavelength and band gap energy. Some of the most common UV-vis phenomena show one or more absorption peaks observed in the UV region, around 260–340 nm. These changes can occur and extend across the spectrum in the visible region, sometimes 360 – 500 nm, even above that range (Cui, Ren, Sun, Liu, & Xia, 2021).

Figure 6 illustrates that the absorption spectrum in the UV-vis range of C-dots, identifies the $\pi \rightarrow \pi^*$ transition of the sp^2 structure at the absorption peak of 275 nm. This transition originates from the conjugated C=C group (Renuga et al., 2025). The absorption band at 322 nm is a prominent band that is associated with the $n \rightarrow \pi^*$ transition, which reaffirms the presence of carbonyl (C=O) groups. This transition

is evidence of graphite formation in C-dots (García-Salcedo, Giraldo-Pinto, Márquez-Castro, & Tirado-Mejía, 2024)

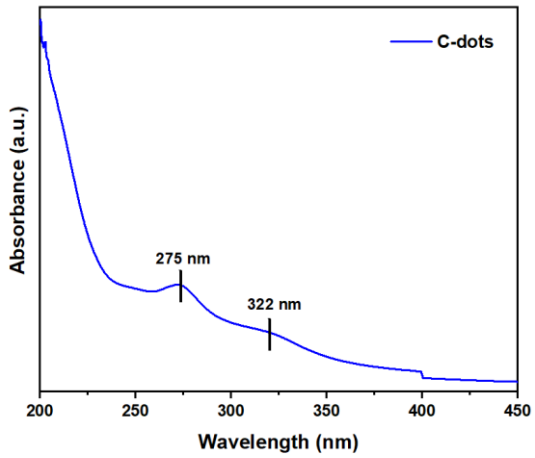

Figure 6. UV-vis spectra of C-dots

Structure Model of C-dots

The C-dots model was hypothesized. This modeling is given to determine the type of bond between urea and d-glucose after passing through the doping process or the addition of nitrogen heteroatoms. The red circles in Figure 7 indicate a simple graphite structure that binds to (CHO), (COOH), NH_3, and O–H (Oliveira et al., 2025).

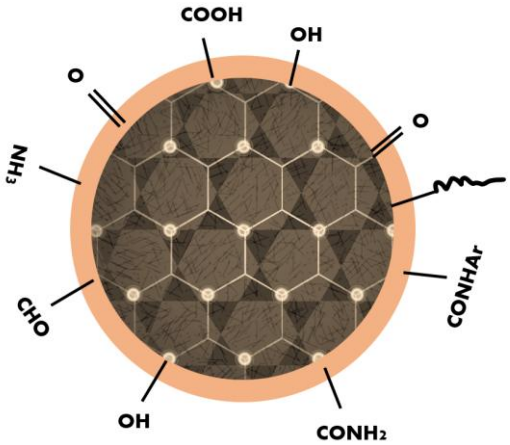

Figure 7. C-dots structure model hypothesis

Amoxicillin Detection

Fluorescence-based C-dot nanomaterials have recently been used to detect AMX. Fluorescence quenching experiments were conducted by adding various concentrations of AMX (10 µM, 15 µM, 20 µM, 25 µM, 30 µM) and adding a 5 µL solution of C-dots to a total solution volume of 10 mL, recording the fluorescence spectrum at a wavelength of 365 nm.

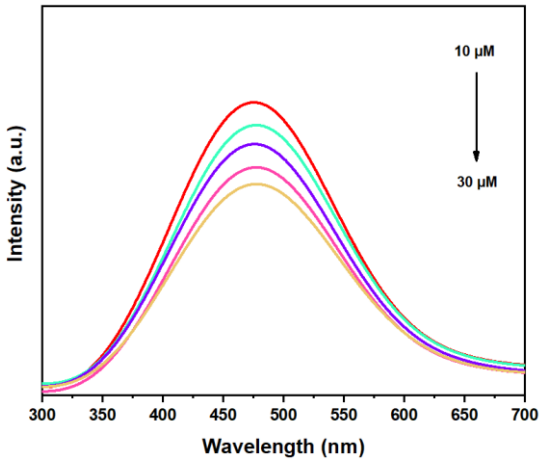

Figure 8. Sensitivity of probe C-dots for AMX detection

The spectra of the maximum fluorescence intensity after adding AMX concentration showed a wavelength at 460 nm (excitation at 365 nm). As the AMX concentration increased from 10 µM to 30 µM, there was a progressive decrease in fluorescence intensity and the intensity was recorded (Figure 8). Specifically, the highest intensity was recorded that showed C-dots with the addition of the lowest AMX concentration (10 µM), while the lowest intensity was observed at the addition of the highest AMX concentration (30 µM). This fluorescence quenching behavior indicates a strong interaction between C-dots and AMX molecules, indicating an efficient electron or energy transfer process.

The emission reduction properties of C-dots after being added to the AMX solution were determined using the Stern-Volmer plot method (Barus, Ginting, Ginting, Ginting, & Emia Pepayosa, 2024). This method is used to observe the relationship between AMX concentration and the intensity ratio of C-dots with various AMX concentrations. The accuracy of sample detection is countinously assessed using the Stern-Volmer method. The equation used to calculate linear regression:

$$\frac{I_o}{I} = 1 + K_{sv}[B] \qquad (3)$$

The peak intensity of the photoluminescence spectrum is the value I and I_o with excitation of 450 nm on all Stern-Volmer plots. Ksv is the Stern-Volmer constant. Then, a linear relationship was established

over the concentration range of AMX (10–30 µM). The fluorescence quenching phenomenon of C-dots is identified with the Stern-Volmer analysis (Kumar et al., 2024). Then, the detection limit was determined using the following equation.

$$LoD = 3{,}3\frac{S_y}{S} \quad (4)$$

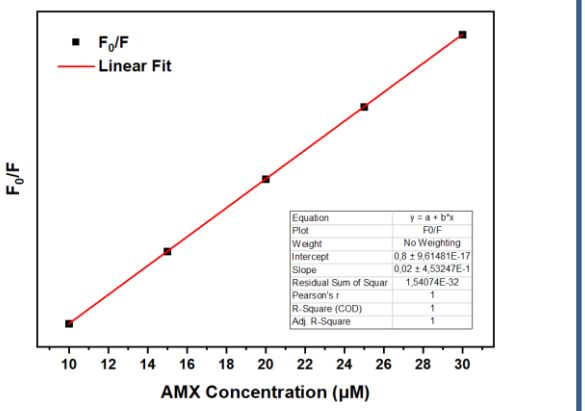

Figure 9. Linear corelation of C-dots for AMX detection

Figure 9 shows a good linear curve. This linear relationship shows a correlation coefficient (R^2) of in this case, Io represents the fluorescence intensity measured without AMX, while I represent the fluorescence intensity observed when AMX was present. Then, the C-dots probe was found to have a LOD of $5{,}75443\times10^{-7}$ nM. This result considered that C-dots have a very high sensitivity to detect the presence of AMX in small concentration. After adding a lot of AMX, nearly all the active areas of the C-Dots are filled up, so the quenching does not get stronger, which makes the N-CDs respond more slowly and become less sensitive. However, when a low amount of AMX is added, it interacts a lot with the surface, leading to strong quenching and a rise in the detection signal or fluorescence intensity (Sanni et al., 2025).

CONCLUSION

The results confirmed that the C-dots exhibited strong blue fluorescence with an emission peak at 440 nm when excited at 365 nm, attributed to surface defect states. Raman analysis indicated the presence of graphitic and amorphous carbon structures. At the sme time, UV-vis spectroscopy revealed characteristic π→π* transition at 275 nm and n→π* transitions at 322 nm, confirming the presence of conjugated C=C and carbonyl (C=O) functional groups. Furthermore, the fluorescence-based detection of AMX was demonstrated, showing a concentration-dependent quenching effect. On the other hand, PL with various excitations shows different fluorescence intensities as a result of quantum effects and surface defects. While other characterizations, PL Decay of N-CDs has a lifetime of 4.09 ns. The Stern-Volmer analysis demonstrated a linear correlation between AMX concentration and fluorescence intensity, yielding a limit of detection (LoD) of 5.75443×10^{-7} nM. This sensitivity is comparable to or better than previously reported C-dot-based AMX detectors, highlighting the potential of these C-dots as a promising fluorescent probe for antibiotic detection.

ACKNOWLEDGMENT

Lembaga Pengelola Dana Pendidikan (LPDP) and Center for Condensed Matter Sciences (NTU Taiwan) were funded and facilitated this research.

REFERENCES

Akbar, S. A., Hasan, M., Nazar, M., Zulfahmi, I., Miswar, E., Iqhrammullah, M., & Jalil, Z. 2025. Fluorescent carbon quantum dots from Syzygium aromaticum as a selective sensor for Fe3+ and Cd2+ detection in aqueous solution. *Case Studies in Chemical and Environmental Engineering*, *11*.

Amin, I. I., Wahab, A. W., Taba, P., Mukti, R. R., Alvin, G., Musa, B., & Azis, H. A. 2025. Indonesian Journal of Chemical Research Hydrothermal Synthesis and Characterization of Sodalite from Feldspar Mesawa Minerals. *J. Chem. Res*, *12*(3), 213–219.

Attia, K. A. M., Nassar, M. W. I., El-Zeiny, M. B., & Serag, A. 2016. Different spectrophotometric methods applied for the analysis of binary mixture of flucloxacillin and amoxicillin: A comparative study. *Spectrochimica Acta - Part A: Molecular and Biomolecular Spectroscopy*, *161*, 64–69.

Barus, D. A., Ginting, A. R. J., Ginting, J., Ginting, R. T., & Emia Pepayosa, B. 2024. Synthesis of Carbon Dots from butterfly pea (Cliptoria ternatea) as detection of the heavy metal ion Cu 2+. *Journal of Physics: Conference Series*, *2733*(1). Institute of Physics.

Barus, D. A., Ginting, R. T., Faizah, A. C., Shafira, R. D., & Nainggolan, K. 2023. Carbon Dots Synthesis from Soybean with Urea Doped As Sensitive Fe (II) Ion Detection. *Indo. J. Chem. Res.*, *10*(3), 171–176.

Cai, Z., Li, Y., Li, J., Zhang, Z., Yang, T., & Yang, S. 2025. Nitrogen-doped carbon quantum dots from pumpkin for the sensing of nifuratel and

temperature. *Spectrochimica Acta - Part A: Molecular and Biomolecular Spectroscopy*, *330*.

Chu, W. X., Tang, X. M., Lu, F. Y., An, B. L., Zhang, J. M., Wang, X. H., Xu, J. 2025. Synthesis of red carbon quantum dots with solvatochromic properties as a selective luminescence probe of MnO4−. *Journal of Photochemistry and Photobiology A: Chemistry*, *463*.

Cui, L., Ren, X., Sun, M., Liu, H., & Xia, L. 2021.. Carbon dots: Synthesis, properties and applications. *Nanomaterials*, Vol. 11. MDPI.

Dali, A., Dali, N., Dali, S., & Amalia, H. A. M. 2021. Synthesis of Glucopyranosyl Acetic from Sago Flour as Raw Material for the Synthetic Polymers. *Indo. J Chem. Res.*, *8*(3), 172–179.

Dimitriev, O., Kysil, D., Zaderko, A., Isaieva, O., Vasin, A., Piryatinski, Y., Nazarov, A. 2024. Photoluminescence quantum yield of carbon dots: emission due to multiple centers versus excitonic emission. *Nanoscale Advances*, *6*(8), 2185–2197.

García-Salcedo, Á. J., Giraldo-Pinto, L. Á., Márquez-Castro, D. J., & Tirado-Mejía, L. 2024. Influence of synthesis parameters on the optical properties of carbon dots. *Carbon Trends*, *17*.

Guo, X. R., Dong, Y. M., Chen, X. Y., & Chen, J. 2022. Sophora japonica L. flower mediated carbon dots with nitrogen and sulfur co-doped as a sensitive fluorescent probe for amoxicillin detection. *Spectrochimica Acta - Part A: Molecular and Biomolecular Spectroscopy*, *282*.

Jessy Mercy, D., Kiran, V., Thirumalai, A., Harini, K., Girigoswami, K., & Girigoswami, A. 2023. Rice husk assisted carbon quantum dots synthesis for amoxicillin sensing. *Results in Chemistry*, *6*.

Jiang, Y., Wang, H., Nie, T., Lu, Y., Zheng, P., Zheng, L., & Zhang, Y. 2025. White-emissive boron and nitrogen co-doped carbon dots for detection of water in organic solvents and Fe3+ ions. *Materials Today Communications*, *44*.

Khairol Anuar, N. K., Tan, H. L., Lim, Y. P., So'aib, M. S., & Abu Bakar, N. F. 2021. A Review on Multifunctional Carbon-Dots Synthesized From Biomass Waste: Design/ Fabrication, Characterization and Applications. *Frontiers in Energy Research*, Vol. 9. Frontiers Media S.A.

Liu, H., Zhong, X., Pan, Q., Zhang, Y., Deng, W., Zou, G., Ji, X. 2024. A review of carbon dots in synthesis strategy. *Coordination Chemistry Reviews*, Vol. 498. Elsevier B.V.

Mallik, A., Hazra, M., Adak, M. K., Nag, R., Pandey, A., & Sahoo, G. P. 2025. Fluorescent probe based on boron-nitrogen co-doped carbon dots for the rapid detection of acephate residue in vegetables and water. *Diamond and Related Materials*, *153*.

Mansuriya, B. D., & Altintas, Z. 2018. Carbon Dots: Classification, Properties, Synthesis, Characterization, and Applications in Health Care-An Updated Review. 11. 1-55

Marpongahtun, Andriayani, Muis, Y., Gea, S., Amaturrahim, S. A., Attaurrazaq, B., & Daulay, A. 2023. Synthesis of Nitrogen-Doped Carbon Dots from Nanocrystalline Cellulose by Pyrolysis Method as Hg2+ Detector. *International Journal of Technology*, *14*(1), 219–231.

Marpongahtun, Gea, S., Muis, Y., Andriayani, Novita, T., & Piliang, A. F. 2018. Synthesis of Carbon Nanodots from Cellulose Nanocrystals Oil Palm Empty Fruit by Pyrolysis Method. *Journal of Physics: Conference Series*, *1120*(1).

Mousa, M. A., Abdelrahman, H. H., Fahmy, M. A., Ebrahim, D. G., & Moustafa, A. H. E. 2023. Pure and doped carbon quantum dots as fluorescent probes for the detection of phenol compounds and antibiotics in aquariums. *Scientific Reports*, *13*(1).

Murugan, B. M., Saleem, S. V. A., Selvan, G. P., Vijayakumar, T. S., Prakash, S., & Murugesan, G. 2025. Synthesis of carbon quantum dots from "De-oiled copra cake" by hydrothermal mechanism: In the realm of bioimaging. *Journal of Pharmaceutical and Biomedical Analysis Open*, *5*.

Oliveira, M. C. D., Silva, A. A., Silva-Silva, T. P., Silva, J. G. V., da Silva Júnior, J. F., Sanchez, D., Santos, F. E. P. 2025. Thermo-optical properties of luminescent carbon dots produced from biomass of Orbignya speciosa (babassu coconut). *Journal of Molecular Liquids*, *423*.

Renuga, V., Vinoliya, X., Dinesh, A., Suthakaran, S., Ayyar, M., Mohanavel, V., … Santhoshkumar, S. 2025. Green synthesis of biocompatible fluorescent carbon dots from bitter gourd for effective metal sensing and biological applications. *Sensing and Bio-Sensing Research*, *47*(100751), 1-6

Sanni, S. O., Bayode, A. A., Brink, H. G., Haneklaus, N. H., Fu, L., Shang, J., & Fan, H.-J. S. 2025. Green Carbon Dots from Pinecones and Pine Bark for Amoxicillin and Tetracycline Detection: A Circular Economy Approach. *Journal of Xenobiotics*, *15*(2), 43-56

Saraswat, V., & Yadav, M. 2020. Carbon Dots as Green Corrosion Inhibitor for Mild Steel in HCl Solution. *ChemistrySelect*, *5*(25), 7347–7357.

Sun, P., Song, W., Zou, Y., Tian, M., Zhang, F., & Chai, F. 2023. The fabrication of N-doped carbon dots by methionine and their utility in sensing Cu^{2+} in real water. *Analytical Methods*, *15*(13), 1631–1638.

Verma, T., Aggarwal, A., Singh, S., Sharma, S., & Sarma, S. J. 2022. Current challenges and advancements towards discovery and resistance of antibiotics. *Journal of Molecular Structure*, *1248*, 131380

Wu, Y., Zeng, L., Zheng, Y., You, F., & Liu, X. 2025. Pectin-derived nitrogen-doped carbon dots as green corrosion inhibitors for N80 steel in 1 M sulfuric acid solution. *Applied Surface Science*, *687*, 162245

Yang, G., & Zhao, F. 2015. Molecularly imprinted polymer grown on multiwalled carbon nanotube surface for the sensitive electrochemical determination of amoxicillin. *Electrochimica Acta*, *174*(1), 33–40.

Yang, J., Wang, Y., & Lu, X. 2025. Efficient room temperature afterglow in nitrogen doped carbon dots triggered by steric hindrance effect. *Journal of Luminescence*, *280*.

Ye, L., Chen, F., Tang, Y., Sun, W., & Song, Y. 2025. Highly selective and sensitive detection of trace amoxicillin with a novel fluorescent nanoprobe N, S-CDs@MIP based on S/N co-doped carbon quantum dots combined with molecularly imprinted polymer. *Journal of Water Process Engineering*, *71*

Zaib, M., Akhtar, A., Maqsood, F., & Shahzadi, T. 2021. Green Synthesis of Carbon Dots and Their Application as Photocatalyst in Dye Degradation Studies. *Arabian Journal for Science and Engineering*, *46*(1), 437–446.